Title
Evaluation of Structural Connectome Models and Network Diffusion in Predicting Cortical Atrophy in Alzheimer's Disease Spectrum

Author
Zhu, Alan

Publication Date
2016

Peer reviewed|Thesis/dissertation

Evaluation of Structural Connectome Models and Network Diffusion in Predicting Cortical Atrophy in Alzheimer's Disease Spectrum

by

Alan Zhu

THESIS

Submitted in partial satisfaction of the requirements for the degree of

MASTER OF SCIENCE

in

Biomedical Imaging

in the

GRADUATE DIVISION

of the

UNIVERSITY OF CALIFORNIA, SAN FRANCISCO

Approved:

[redacted]

Dedication & Acknowledgments

I dedicate this publication and all related work first and foremost to my thesis advisor Dr. Duygu Tosun-Turgut. Thank you for your willingness and commitment to always teach me about brains, medicine, and mathematics. Thank you for not only helping me to maintain healthy expectations of research and of myself, but also for having persistent faith that I can achieve anything I want to achieve.

I give my deepest sense of appreciation and gratitude to the outstanding members of my steadfast thesis committee, Dr. Christopher Hess, Dr. Dieter Meyerhoff, and Dr. Duan Xu. Thank you all for taking the time to invest in and enlighten me with insightful opinions, authentic encouragement, and constructive criticisms to help me grow as a researcher, student, and human being.

This work is heavily inspired by the work of Ashish Raj, associate professor of neuroscience at Cornell University. Though we have never met face to face, thank you Dr. Raj for your contributions to the fields of biomedical imaging and neuroradiology that have allowed for the motivation and existence of this thesis.

Last but certainly not least to be considered, I want to give a huge shout out to all of my classmates, the Masters of Science in Biomedical Imaging (MSBI) class of 2016. In particular, I'm grateful to Vishal "Vish" Samboju and Xinheng "James" Zhang, for their brotherly loyalty, love, and support. This past year was bright, memorable, and absolutely hilarious because I got to walk alongside each and every one of you.

To all those aforementioned I am forever indebted.

Thanks!

Evaluation of Structural Connectome Models and Network Diffusion in Predicting Cortical Atrophy in Alzheimer's Disease Spectrum

Alan Zhu

Abstract

Alzheimer's Disease (AD) is one of the most common forms of dementia, yet the exact mechanisms by which it operates and progresses through the brain are not completely known. To help identify and characterize the underlying pathways, or subnetworks, of AD, a network diffusion model is built based on the heat diffusion equation, grey matter volume atrophy measurements, and individual brain structural connectivity networks. Longitudinal neuroimaging data from individuals in various stages of the AD disease spectrum are used to seed the model as well as provide empirical end-atrophy measurements to assess overall model predictive value. The dominant brain networks facilitating AD progression in each patient are extracted using regression analysis and these principal networks are then clustered into distinct groups by applying dimensionality reduction and classification. These identified groups expose AD-specific subnetworks, each having a unique distribution of disease spread topology through various regions of the brain. Further anatomical evaluation of these subnetworks shows that the affected regions of interest coincide with and support long-standing results of previous research.

Table of Contents

List of Tables

List of Figures

List of Equations

1 Introduction

Alzheimer's Disease (AD) is a progressive neurodegenerative disease that affects roughly 48 million people worldwide. It is the most common form of dementia, accounting for 60-70% of all cases [5]. Clinical symptoms of sporadic AD usually begin in elderly individuals over 65 years of age and initially present with short-term memory loss. Life expectancy after diagnosis is 8-10 years on average with advancement of the disease leading to neurological symptoms of increasing severity as well as loss of motor and other critical bodily functions [6]. Classified as a proteopathy, i.e. a disease caused by abnormal protein structure, AD results from accumulation of misfolded amyloid beta and tau proteins in the brain [8]. The exact path from this protein buildup to the onset of the disease remains a present area of research.

A critical component in understanding and developing treatment for AD lies in understanding how the disease progresses and spreads in terms of structural brain changes, as a surrogate measure of underlying neurodegeneration. AD advances in a trans-synaptic manner, moving along various structural networks in the brain [15]. AD associated neurodegeneration pattern is highly stereotyped, beginning in the medial temporal lobe, spreading next to the lateral temporal and parietal lobes, and eventually making its way to the frontal and occipital lobes [11]. In addition, research strongly suggests that AD attacks brain regions in accordance to function as opposed to physical proximity, thus incorporating understanding and modeling of the brain's structural and functional connectivity has become necessary for the advancement of AD research.

Raj et al. (2012, 2015) present a "network diffusion" model that aims to mathematically model the spread of AD-related pathophysiology mediated by and restricted to the brain's intrinsic structural connectivity networks measured from diffusion-weighted magnetic resonance imaging (MRI) [12,13]. The premise behind this approach is that in light of accumulating evidence for the trans-

neuronal transmission of AD, the spread pattern of AD pathophysiology may be mathematically modeled to predict individual disease progression based on baseline measurements. A simple mathematical model based on heat diffusion is proposed and its predictive results are reproduced in Figure 1a.

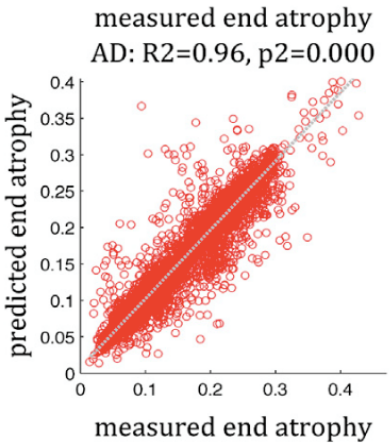

Figure 1a: Atrophy predicted by network diffusion model plotted against actual observed atrophy [reproduced from Raj et al. (2015)]

Inspired by these preliminary findings, this investigation examines the work of Raj et al. (2015) and evaluates the predictive power of the network diffusion model and its ability to capture the spatiotemporal evolution of neurodegeneration in the AD disease spectrum. This study seeks to further existing research by attempting to characterize both the diffusion model and the disease spread at finer granularity, using longitudinal model fitting to extract the subnetworks influencing AD progression. It primarily considers observations in subject grey matter atrophy patterns and subject brain connectivity models called connectomes. Long-term atrophy measurements derived from longitudinal structural MRIs are used as a surrogate measure of regional neurodegeneration spread.

Previous research does not take into account the specific networks facilitating the spread, but rather considers the disease as a whole, focusing on end-atrophy prediction. This work employs various methods of mathematical analysis in attempt to identify these specific individual networks. Via eigen decomposition of subject connectomes and application of partial least squares regression, the dominating networks capturing the disease spread are identified and isolated. By successively applying dimensionality reduction and classification techniques, clear and identifiable patterns and categories can be observed amongst various network paths. At certain points in the investigation

where applicable, limitations of the original proposed model and results are identified and addressed.

2 ADNI MRI Data Processing

Data used in this study were obtained from the Alzheimer's Disease Neuroimaging Initiative-2 (ADNI-2) database (www.adni-info.org). Led by principal investigator Michael W. Weiner, MD, ADNI was launched in 2003 as a public-private partnership. The primary goal of ADNI has been to test whether serial magnetic resonance imaging (MRI), positron emission tomography (PET), various biological markers, and clinical and neuropsychological assessment can be used in combination to measure the progression of mild cognitive impairment (MCI) and early Alzheimer's disease (AD) in clinical trials [3].

2.1 MRI Scan Protocols

All subjects underwent whole-brain MRI scans on 3 Tesla GE Medical Systems scanners at 14 acquisition sites across North America. Anatomical T1-weighted images from spoiled gradient echo sequences (SPGR, 256 × 256 matrix; voxel size = 1.2 × 1.0 × 1.0 mm^3; TI = 400 ms; TR = 6.98 ms; TE = 2.85 ms; flip angle = 11°), and diffusion-weighted images (DWI; 256 × 256 matrix; voxel size: 2.7 × 2.7 × 2.7 mm^3; TR = 9000 ms; scan time = 9 min) were collected. 46 separate images were acquired for each DTI scan: 5 T2-weighted images with no diffusion sensitization (b0 images) and 41 diffusion-weighted images (b = 1000 s/mm^2). This protocol was chosen after conducting a detailed comparison of several different DTI protocols to optimize the signal-to-noise ratio in a fixed scan time. All T1-weighted MRI and DWI images underwent visual inspection for quality assurance to exclude scans with excessive motion and/or artifacts. No scans were excluded.

2.2 Structural MRI processing

FreeSurfer is an open source software suite for automated analysis of human brain MRI data (http://surfer.nmr.mgh.harvard.edu/fswiki). FreeSurfer 5.3 was used to estimate regional atrophy in terms of total grey matter tissue volume for 84 cerebral cortical and subcortical brain regions. Each of these is referred to as a specific region of interest or ROI. Each cortical ROI is associated with one of four lobes: frontal, occipital, parietal, or temporal. ROIs pertaining to the cerebellum were not included in these analyses.

To reduce the confounding effect of intra-patient morphological variability, each participant's longitudinal data series was processed by longitudinal stream processing in FreeSurfer [14]. For each patient FreeSurfer calculates a median template brain and resamples all data points accordingly, allowing for joint processing of data from all scan sessions. FreeSurfer longitudinal processing also ensures consistent ROI definitions and minimal measurement errors within each subject over multiple time points. All images underwent standardized quality control procedures. Participants with complete segmentation failure or gross errors throughout all brain regions were rated as complete failure and those with gross errors in one or more specific brain regions (i.e., temporal lobe regions, superior regions, occipital regions, and insula) were given a partial pass rating. All subjects included in this study received a complete pass rating.

2.3 Diffusion-Weighted MRI Processing

Each subject's raw DWI volumes was aligned to the average b0 image (DTI volume with no diffusion sensitization) using the FSL **`eddy_correct`** tool to correct for head motion and eddy current distortions. To correct for echo-planar imaging (EPI) induced susceptibility artifacts which can cause distortion at tissue–fluid interfaces, skull-stripped b0 images were linearly aligned (FSL *FLIRT* 9 dof) and then elastically registered to their respective T1-weighted structural scans using an inverse-

consistent registration algorithm with a mutual information cost function as described by Jahanshad et al. (2010) [7]. The resulting 3D deformation fields were then applied to the remaining 41 DWI volumes prior to estimate diffusion parameters. To account for the linear registration of the DWI images to the structural T1-weighted scan a corrected gradient table was calculated. A single diffusion tensor, or ellipsoid, was modeled at each voxel in the brain from the eddy and EPI-corrected DWI scans using FSL **`dtifit`**. The DTI tensor model has its limitations, particularly in regions where fibers cross, but is not investigated further here.

2.4 Connectome Processing

Connectomes represent the structural connectivity networks in the brain. In their graphical representation, labeled ROIs are nodes and streamlines between regions are undirected edges connecting some or all pairs of nodes. Using this graphical definition, connectome data can be represented by an adjacency matrix, where the dimensions are both equal to the number of ROIs and the value at entry *(i,j)* is equal to the number of tracks between ROI or node *i* and *j*. Since track direction is not considered in these analyses the adjacency matrix is symmetric, i.e. the value at *(i,j)* is equal to the value at *(j,i)*.

Camino (http://camino.cs.ucl.ac.uk/) is an open-source software toolkit developed for diffusion MRI processing and is used for purposes of this investigation. Deterministic streamline tractography is performed via Camino's **track** command, utilizing directional information derived from the diffusion tensor and the 84 ROIs defined by FreeSurfer. The 84 FreeSurfer ROIs and corresponding set of tracts are used as inputs into the **conmat** command from Camino which reads the target image containing the labeled ROIs and streamlines output by tract. **conmat** generates a matrix counting the number of streamlines connecting each pair of ROIs in the target image.

3 Study Cohort

ADNI recruits volunteers that commit to providing their own diagnostic information over a multi-year timespan to contribute towards AD research. All subjects analyzed had both diffusion-weighted and structural MRIs at baseline and at least one follow-up structural MRI. Subject diagnoses span the AD spectrum with the following categories: early mild cognitive impairment (EMCI), late mild cognitive impairment (LMCI), and Alzheimer's Disease (AD). Clinical diagnoses were based on natural history and cognitive assessment and were not validated using histopathology or imaging.

This study analyzes data from 53 patients, divided into 3 groups based on diagnosis of either EMCI, LMCI, or AD, and 110 subjects categorized as cognitively normal (CN), used as a control group. Cross-sectional (i.e., study baseline) regional grey matter volume estimates for CN subjects are used to create normal population distribution (i.e., mean and standard deviation) for each ROI. Estimated regional normal population distributions are used to standardized grey matter volume estimates from longitudinal structural MRIs to z-scores for the 3 patient groups (cf. Section 3.3 Z-Score Conversion). Patients with subjective memory complaints (SMC) are normally also included in the AD spectrum, but the selected cohort contained only 2 SMC subjects, who were excluded to preserve statistical confidence and significance.

The ADNI study population is well balanced with regards to age, gender, and other subject characteristics. The subcohort examined here were selected without any consideration to these factors as specific population comparisons are not within the scope of this investigation.

3.1 Cohort Data

All subject data, including connectome data, ROI volume measurements, subject diagnoses, and ROI lobular region mappings, were provided in CSV and XLS format. All data analysis was

performed using MATLAB R2015a. Raw data was imported via native MATLAB data import library functions **csvread** and **xlsread**. Each subject was represented as a **struct** data type in MATLAB, and the entire cohort as an array of **struct**. Table 3.1a describes a selection of these **struct** fields.

Table 3.1a: Description for select fields within each subject's **struct** element.

Field	*Data Type*	*Description*
connectome	*84x84 double*	*Matrix of connectivity strength between each ROI*
eigenvalues	*83x1 double*	*Eigenvalues from the eigendecomposition of the connectome matrix* *Note: Eigenvalues are thresholded to zero if below =10-5, so the original eigenvalue vector from 84 ROIs is trimmed from length 84 to 83.*
eigenvectors	*84x83 double*	*Eigenvectors corresponding to each eigenvalue, arranged columnwise*
volume_data	*Nx84 double*	*Grey matter volume measurements for each ROI, with each column representing one ROI and each row representing one scan session/time point*
icv	*Nx1 double*	*Intracranial volume, one measurement taken per scan session/time point*
time_points	*Nx1 double*	*Array of decimal values corresponding to the number of years from the baseline scan to each scan session*
dx	*string*	*Subject diagnosis, one of 'EMCI', 'LMCI', or 'AD'*

3.2 Time Point Scaling

Subject scan dates were initially logged and provided in mm/dd/yyyy format. For each subject the scan date was parsed and converted into MATLAB serial form as defined by the function **datenum**, representing the number of whole and fractional number of days from January 0, 0000 in the proleptic ISO calendar (http://www.mathworks.com/help/matlab/ref/datenum.html). Each serialized scan date was then normalized via Equation 3.2a. This creates a year-based decimal time scale (1 year = 1.0) that can be easily plotted or used as a vector. The baseline scan is set to a value of 0, and every subsequent scan becomes a decimal value corresponding to the number of years between the scan date and the baseline scan date.

Equation 3.2a: Time point normalization for scan dates

$$\frac{\boldsymbol{datenum}(scan\ date)\ -\ \boldsymbol{datenum}(baseline\ scan\ date)}{365}$$

3.3 Z-Score Conversion

The volumetric data obtained from the scans was initially provided in mm^3, with values on the order of 10^6 in magnitude. As noted earlier, FreeSurfer longitudinal stream processing minimizes *intra*-subject measurement error over time, but in order to account for *inter*-patient discrepancies, as well as reduce computational complexity, volumetric measurements were converted to z-scores prior to all analyses.

To convert all data points to z-scores, 110 cognitively normal (CN) subjects were used. A control mean and standard deviation were calculated for each ROI by averaging each ROI volume at each control subject's individual time points across all subjects. Before averaging, the ROI volumes were normalized within each subject by taking each subject's baseline ROI volume from each scan and dividing by the baseline intracranial volume (ICV). ICV is an approximate representation for total brain volume and FreeSurfer uses template-based estimation to calculate this, as opposed to simply taking a summation of all regions. After normalization, every volume measurement in the analysis cohort was then remapped by means of the standard z-score equation given by Equation 3.3a. Here mu and sigma represent the mean and standard deviation calculated from all the control measurements for a given ROI.

Equation 3.3a: z-score conversion for subject volume measurements

$$z_{roi} = \frac{x_{roi} - \mu_{control\_roi}}{\sigma_{control\_roi}}$$

4 Methods

4.1 Eigen Decomposition

As a first step to characterizing the diffusion network in the brain, the eigen decomposition of each subject's connectome is considered. Each subject's connectome is a symmetric square matrix having a dimension equal to the number of ROIs, i.e., 84x84. The eigen decomposition of each connectome yields a vector of length 84 corresponding to the connectome eigenvalues, and a square matrix of dimension 84x84 representing 84 eigenvectors, each of length 84 concatenated column-wise into a matrix according to the eigenvalue ordering. Conceptually, the eigenvectors (i.e., 84x1 vector) represent the orthogonal sub-networks of brain connectivity, and the eigenvalues relate to the natural frequencies of the associated connectivity patterns (i.e., eigenvectors) emerging on the particular connectome.

To observe patterns in the eigenvalues across subjects, the eigenvalues for each subject are bucketed and visualized via MATLAB's **`histogram`** function. Additionally, sorting each subject's eigenvalues in numerically ascending order and plotting for all subjects gives a more continuous representation where the slope and curvature of the line reveal information about the eigenvalue distribution across subjects. As an additional step to reduce noise in the results, thresholding is applied to zero out any eigenvalues of insignificant but nonzero magnitude. Any eigenvalues below the thresholding limit of $\varepsilon = 10^{-5}$ are removed, as well as their corresponding eigenvectors. Consequently, patients may have eigenvector matrices that are not square, e.g. 84x83 if one eigenvalue is removed. The histogram and plot of sorted eigenvalues are illustrated in Figure 4.1a and Figure 4.1b respectively. Each color represents the data set for an individual subject.

Figure 4.1a: Histogram of eigenvalues for all subjects

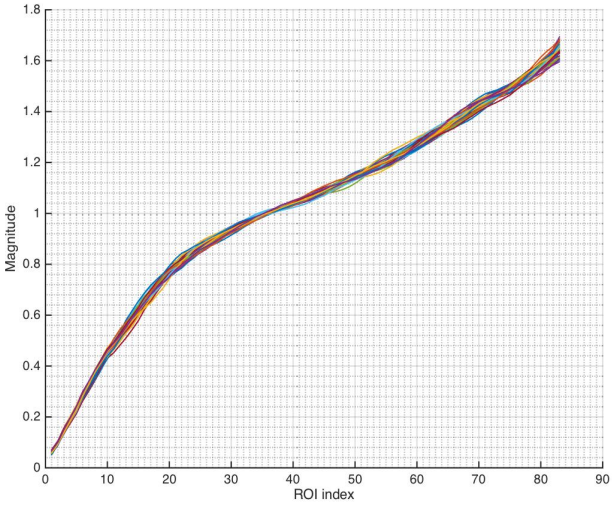

Figure 4.1b: Sorted eigenvalues for all subjects

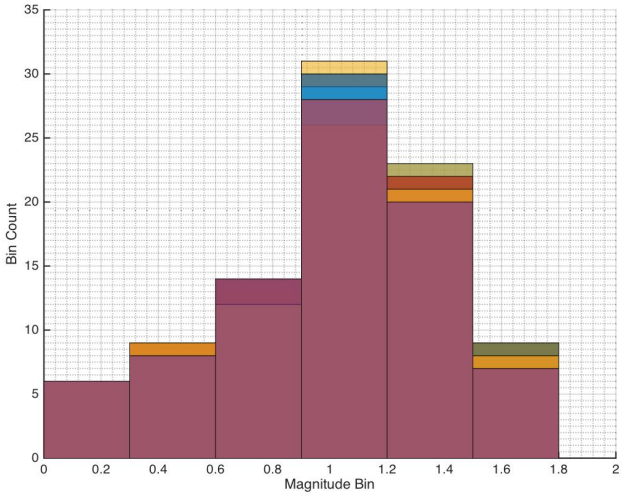

4.2 The Network Diffusion Model

The network diffusion model proposed by Raj et al. (2015) to predict spread and magnitude of neurodegeneration progression by attempting to fit subject atrophy to a deterministic mathematical model. The basis of the model is of the form described in Equation 4.2a., where the disease pattern at time *t* is essentially characterized as the multiplication of a diffusion "kernel" or "filter", $e^{-\beta Ht}$, into the baseline volume or baseline atrophy measurements. Here *H* represents the network Laplacian derived from the subject connectome matrix, β a diffusion speed coefficient, X_0 the baseline atrophy pattern, and *t* the time elapsed since the baseline measurement. Note that in the context of the network diffusion model, baseline atrophy refers to the grey matter tissue volume observed at the initial study visit, and end-atrophy refers to the grey matter tissue volume from the subject's follow-up scans.

Equation 4.2a: Basic network diffusion model proposed by Raj et al. (2015)

$$\mathbf{x}(t) = e^{-\beta Ht}\,\mathbf{x}_0,$$

Recall the results obtained by Raj et al. (2015) from plotting the model predicted end-atrophy against observed actual end-atrophy in Figure 1a. The plot displays a strong, positive linear correlation between predicted and observed end-atrophy and adherence to the *y=x* line of symmetry, which represents the line where predicted end-atrophy directly equals observed end-atrophy. The source code developed by Raj et al. (2015) was dissected to validate the methods used in producing these results and revealed the following general algorithm:

I. For each ROI, take the first and last volume measurements. These are the baseline scan volume data and the most recent scan follow-up volume data. This yields 2 84x1 vectors.

II. Define a range for the model time *t*, namely a linearly spaced vector from 0 to some maximum value.

III. For each time point *t* in this vector, do the following:

   A. Calculate a vector according to the network diffusion model equation for disease evolution. Expanding the basic network diffusion model equation gives Equation 4.2b where disease evolution is then based on the eigen decomposition of the connectome.

   Equation 4.2b: Network diffusion model rewritten in terms of eigenvalues and eigenvectors (Raj et al., 2015)

$$\mathbf{x}(t) = Ue^{-\Lambda\beta t}U^{\dagger}\mathbf{x}_0 = \sum_{i=1}^{N}\left(e^{-\beta\lambda_i t}\mathbf{u}_i^{\dagger}\mathbf{x}_0\right)\,\mathbf{u}_i.$$

   Here *U* represents the eigenvector matrix, Λ represents the eigenvalue vector, and u_i, λ_i represent the i^{th} eigenvector and eigenvalue, respectively.

   B. Correlate the resulting model vector from **A.** with the end-atrophy vector in **I.** and store the correlation coefficient for point *t*.

IV. Pick the point *t* with maximum correlation coefficient as the end model time, t_{max}.

This point, t_{max} now represents the "time" point that gives the model the best correlation between predicted end-atrophy calculation and the true end-atrophy observation. Note the time

range of the model is a variable unique for each subject, so the range and spacing of t the model operates on is separate from real absolute time. Since t_{max} defines the model time where the model best predicts the observed end-atrophy, t_{max} can be converted into real time by aligning it to the scan date of the end-atrophy scan. Finally, re-substituting it into the network diffusion model equation yields the model-predicted end-atrophy measurement itself. The plot from Raj et al. (2015) plots exactly this value against the observed end-atrophy.

4.3 Partial Least Squares Regression

Connectomes and their eigen decomposition give a general map of the diffusion network across each subject's brain. The eigenvectors, also referred to as "eigenmodes" in the context of network diffusion, give a sense of how strong the diffusivity and connectivity is between any pair of ROIs. In the results published by Raj et al. (2015), each eigenmode is given equal weight in facilitating the diffusion (i.e., spread) of the initial atrophy pattern. But research has shown AD spreads across the brain's neural network in a non-uniform fashion and likely spreads unevenly across the neuronal pathways of the brain. The distribution of the eigenvalues shown in Figure 4.1a and Figure 4.1b further support the theory that not all the network regions across the brain diffuse uniformly, and so in addition each eigenmode possessing its own eigenvalue "magnitude," the AD pathology spread may be determined by a separate specific weighting applied across the subject's eigenmodes.

Partial least squares regression, or PLS regression, is a statistical method combining principal component analysis and multiple regression that can be used to find the underlying relationships between two given matrices. PLS regression proves particularly effective in situations where the number of "predictors," or input variables, far exceeds the number of observations. In this context the 84 ROI eigenmodes represent the predictor variables, and the longitudinal grey matter volumetric measurements for each ROI are the observations.

PLS is a linear regression model, so given as input both the end-atrophy observation vector and the model-atrophy matrix at a time point *t*, PLS will find the best linear combination of coefficients that relate the model matrix to the end-atrophy measurements. For each instance of PLS, the resulting linear combination can then be multiplied into the model matrix and correlated with the end-atrophy observation as before to produce a regression coefficient that gives an overall metric of predictive strength. Because the model is re-evaluated at each time point *t*, a separate PLS regression is done for every time point *t*, and t_{max} is then defined by the time point that produces the PLS coefficients having the highest correlation with the true atrophy measurements.

4.4 t-SNE Dimensionality Reduction

Classification needs to be done in order to better group and characterize the various patterns amongst the subject eigenmodes. The t-distributed stochastic neighbor embedding (t-SNE) dimensionality reduction technique is used to map each subject's 84 variable eigenmode vector to a 2-dimensional space. t-SNE is based off stochastic neighbor embedding and specialities in visualizing high-dimensional data in 2D or 3D space (van der Maaten, 2014) [17]. The implementation used here was provided as a MATLAB library (https://lvdmaaten.github.io/tsne/).

t-SNE, unlike PCA or other dimensionality reduction methods, has a non-convex objective function. The objective function is minimized using a gradient descent optimization seeded randomly with the default perplexity parameter value (van der Maaten, 2014) [17].

4.5 *k*-means Classification

k-means classification is an unsupervised classification method where the number of desired clusters *k* is given, and elements are classified into *k* clusters based on minimizing Euclidean distance from an average centroid or mean of every cluster.

5 Analysis and Results

5.1 Accuracy and Limitations of t_{max}

Raj et al. (2015) showed that using the implementation of the diffusion model as described in the previous section yields a plot of model versus empirical end-atrophy well defined along the line of symmetry $y = x$ showing that the model, at some scaling defined by t_{max}, can produce an end-atrophy value very close to the observed end-atrophy from real subjects. However, after applying the identical algorithm to the subject data for this investigation, a histogram of t_{max} across all subjects reveals that all t_{max} have values at or close to zero. This means that the model values at t=0 produced the highest correlation with the observed end-atrophy values. Since the model at t=0 is identical to the initial observed baseline atrophy ($e^{-\beta Ht}$ filter goes to 1), this means the baseline atrophy is closer to the end-point than any calculation produced by the model, giving it effectively zero predictive value. Algorithmically speaking, this means the largest model-predicted values (smallest t, least atrophy, highest remaining volume) have the highest correlation with the observed-end atrophy. Thus the kernel is decaying much faster than the true state of the disease and the floor of the range of t is most likely too large to produce any useful model.

In an attempt to mitigate this problem, the range of t is adjusted to lower values. But if the range is set too low, t_{max} then aggregates all at the end of the range, or the maximal value of t. When the t_{max} distribution is skewed towards the maximal value of t it indicates the values of t are too large to properly reflect the true diffusion rate across ROIs. Algorithmically speaking, this means the smallest model predicted values (largest t, greatest atrophy, lowest remaining volume) have the highest correlation with the observed end-atrophy, meaning the model decays too slowly compared to the true state of the disease and the max value of t in the given range is still insufficient to provide a useful model.

It turns out there is no "sweet spot" for the range of *t* in terms of the pre-existing out-of-the-box implementation. Since finding an accurate range for *t* is critical to the predictive accuracy of the model, the plots presented in Raj et al. (2015) do not accurately reflect the power of the model they imply, at least not in a straightforward manner. A primary goal then becomes modifying the model in attempt to correct the t_{max} distribution. The mathematical equation for describing the disease atrophy is reconsidered and partial least squares regression is applied to each subject's eigenvectors.

5.2 Reformulating the Network Diffusion Model

The atrophy seen from the MRI data, i.e. the reduction in grey matter volume per ROI, is the primary measurement upon which the model results are based. As noted previously, the simulation provided by Raj et al. (2015) was initially coded with the mathematical equation for the AD disease pattern described in Equation 4.2b, but that equation does not account for accumulation of the disease. The input data in this context, however, is in terms of volumetric measurements, which needs to be interpreted exactly as pathological accumulation. So taking an integral over the basic original equation gives a formulation for pathology accumulation, and thus provides the proper equation for describing the model-predicted atrophy and for the input subject data. Equation 5.2a shows the derivation of the reformulated equation.

Equation 5.2a: Network diffusion model in terms of accumulated pathology or volume loss (atrophy) (Raj et al., 2015)

$$\begin{aligned}\boldsymbol{\Phi}(t) &= \int_0^t e^{-H\beta t}\mathbf{x}_0\, dt = U\frac{1}{\beta}\Lambda^{-1}\left(I - e^{-\Lambda\beta t}\right)U^{\dagger}\mathbf{x}_0 \\ &= U\, diag\left(\left\{\begin{array}{ll} t, & i=1 \\ \dfrac{1-e^{-\lambda_i\beta t}}{\beta\lambda_i}, & i>1 \end{array}\right\}\right)U^{\dagger}\mathbf{x}_0.\end{aligned}$$

Although the above derivation is published in the results of Raj et al. (2015), the code used to generate the published results relies only on the initial disease progression equation described in Equation 4.2b, perhaps due to the format of input subject data and for purposes of providing an initial simplified proof-of-concept. Since this study uses multi-year longitudinal MRI atrophy measurements, Equation 5.2a is substituted as the basis for all further analysis.

Modification of the network diffusion equation alone proves insufficient to shift t_{max} away from zero, meaning that there are still significant factors in the disease spread behavior the model still hasn't accounted for. After modifying the network diffusion equation to Equation 5.2a and incorporating PLS into the t_{max} selection algorithm, the t_{max} distribution becomes much more centralized and neither skewed towards zero or the end of the range of t. This makes for a much stronger argument for the power and accuracy of network diffusion model because the range of t reasonably reflects the true rate of atrophy displayed by the empirical data. t_{max} is no longer inaccurately skewed towards zero or the maximum value of t meaning the model can now produce a correlation that surpasses the bias of baseline atrophy and end-atrophy measurements. Figure 5.2b shows the distribution of t_{max} after implementing the new diffusion model equation and PLS regression.

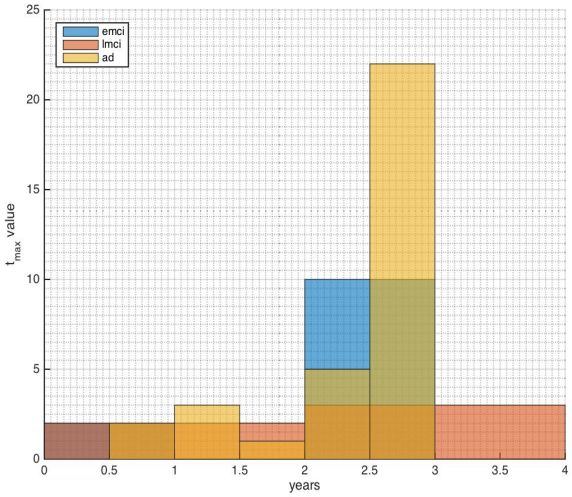

Figure 5.2b: Histogram of t_{max} after model improvements

5.3 Principal Eigenmodes

Previous evaluation of subject eigenvalue histograms showed a small number of eigenvalues having small magnitude, and a majority of eigenvalues having large magnitudes. Factoring in the

kernel of the network diffusion model $e^{-\lambda_i}$, the model implies that a large number of eigenvalues diffuse very quickly (large lambda, faster decay), and a small number of eigenvalues diffuse slower over time (small lambda, slower decay) and so end up dominating the diffusion process. Consequently, if this hypothesized behavior stands true then the histogram of the optimized (t_{max}) PLS coefficients across all subjects should reflect this. The majority of PLS coefficients should remain similar in value, with only a few that are outliers, indicating the dominant eigenmodes. To confirm this, for each subject the PLS coefficients for the model at t_{max} are converted to z-scores and absolute values of the z-scores across all subjects are histogrammed, with the resulting visualization shown in Figure 5.3a.

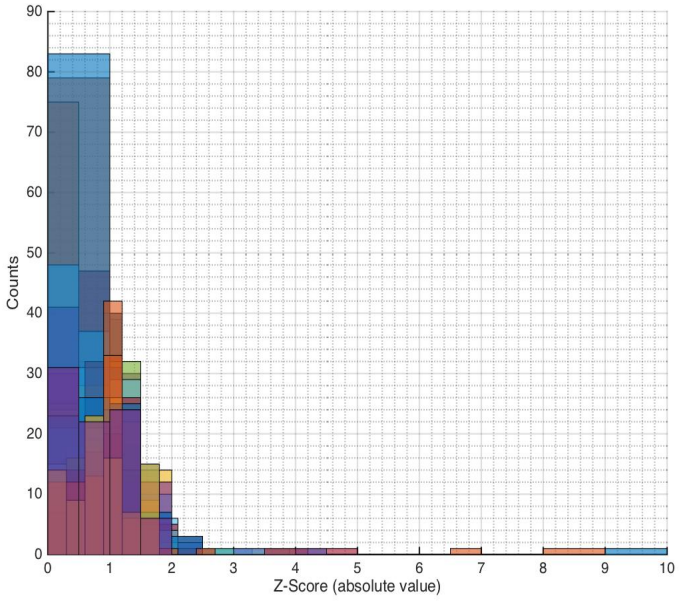

Figure 5.3a: Histogram of z-scored PLS coefficient magnitude across all analyzed subjects

The PLS coefficient histogram shows a distribution that supports the implications of the model and eigenvalue distribution. The distribution follows an inverse power law relationship, where the PLS coefficient weights are heavily concentrated in only a few eigenmodes, if not a single one. Because these "principal" eigenmodes dominate the spread of the disease the scope of any further analysis will be limited to these principal eigenmodes and removes the other eigenmodes from consideration.

As an additional point of analysis, the distribution of principal eigenmodes as a function of eigenvalue index is evaluated. For each subject, the principal eigenmode determined by PLS corresponds to an eigenvalue. Recall from Table 3.1a that for each subject the eigenvalues are

stored in sorted order, so for each subject the rank of the principal eigenmode is collected and the indices of the principal eigenmodes across all subjects are histogrammed. Examining Figure 5.3b almost half of the study subjects had a principal eigenmode corresponding to the first or smallest eigenvalue. This supports the intuition behind the network diffusion model that smaller eigenvalues tend to dominate the pathology spread.

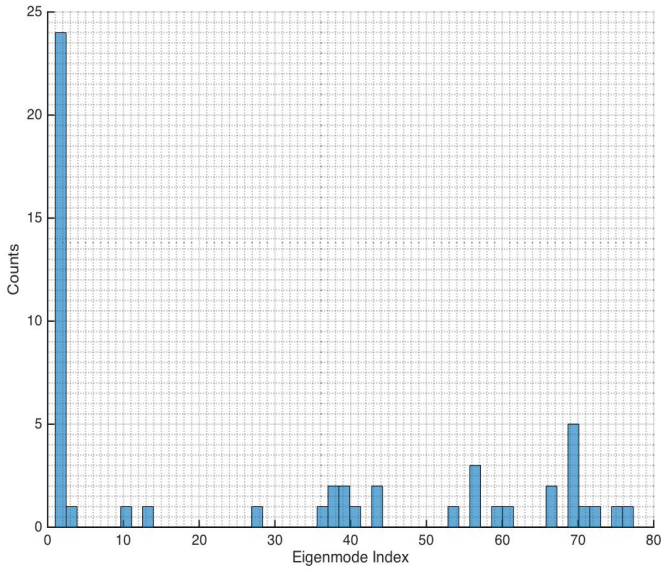

Figure 5.3b: Histogram of the indices for the principal eigenmodes across all analyzed subjects

5.4 ROI-based Inspection

In the context of the network diffusion model, the principal eigenmodes represent the main subnetworks by which AD pathology progresses. Having identified these, it becomes important to characterize these subnetworks, looking for patterns and consistencies in the dominant eigenmodes across subjects. Similarities across these networks may indicate pathways of disease preference, or groupings of eigenmodes may be linked to disease stage or subject-specific similarities and differences.

As an initial step in characterizing the principal eigenmodes, the principal eigenmodes for all subjects are plotted together, yielding the “spectra” seen in Figure 5.4a. Each colored line represents the principal eigenmode for one subject, with the normalized value of each ROI plotted against the ROI index. This visualization yields little information, as the eigenmodes seem to have no relation to each other, appearing much like noise or completely independent variables.

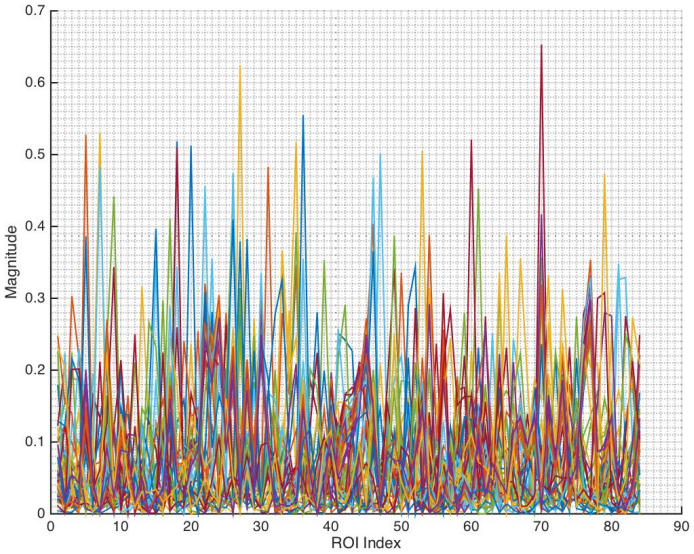

Figure 5.4a: Plot of normalized principal eigenmodes across all subjects

However, if the ROIs are grouped by lobular region and then plotted, much more distinct patterns are noticeable. Figures 5.4b and 5.4c show only the ROIs of the principal eigenmodes located in the frontal and temporal regions, respectively. Realizing these patterns within each ROI is useful in the sense that it confirms there are similarities between the principal eigenmodes and motivates the need for classification or clustering. However, because the nature of the disease spreads from one region to another, the eigenmodes still require to be classified in their entirety, so the ROI-based inspection is limited to this point.

Figures 5.4b & 5.4c (left & right): Principal eigenmodes limited to ROIs located in the frontal (b) and temporal (c) lobes.

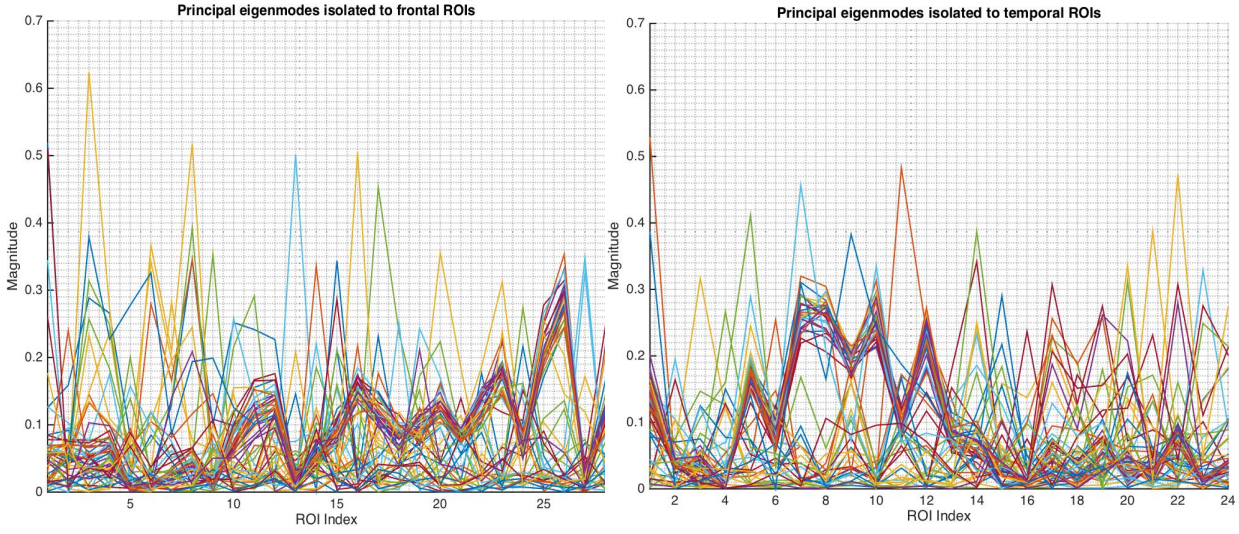

5.5 Dimensionality Reduction & Classification

In order to classify the principal eigenmodes, the dimensionality of the eigenmodes needs to be reduced. The data consists of 84 ROIs which effectively represents 84 dimensions but the

number of subjects is less than the number of ROIs, namely 53, so the dimensionality is actually limited at 53. The output of t-SNE in 2D space can be seen in Figure 5.5a.

After dimensionality reduction, *k*-means clustering is used to classify the 2D eigenmode vector data. The cluster number *k* was not optimized but cluster distinction diminished significantly after *k=3*. Figures 5.5b and 5.5c show the output clusters and centroids. The resulting clusters show no apparent correlation with progression or stage of the disease - each cluster had similar proportions of EMCI, LMCI, and AD subjects. Note for Figures 5.5a, 5.5b, and 5.5c, the axes are unitless and simply serve to represent the new *n* (where *n=2,3*) dimensional space the data has been mapped onto.

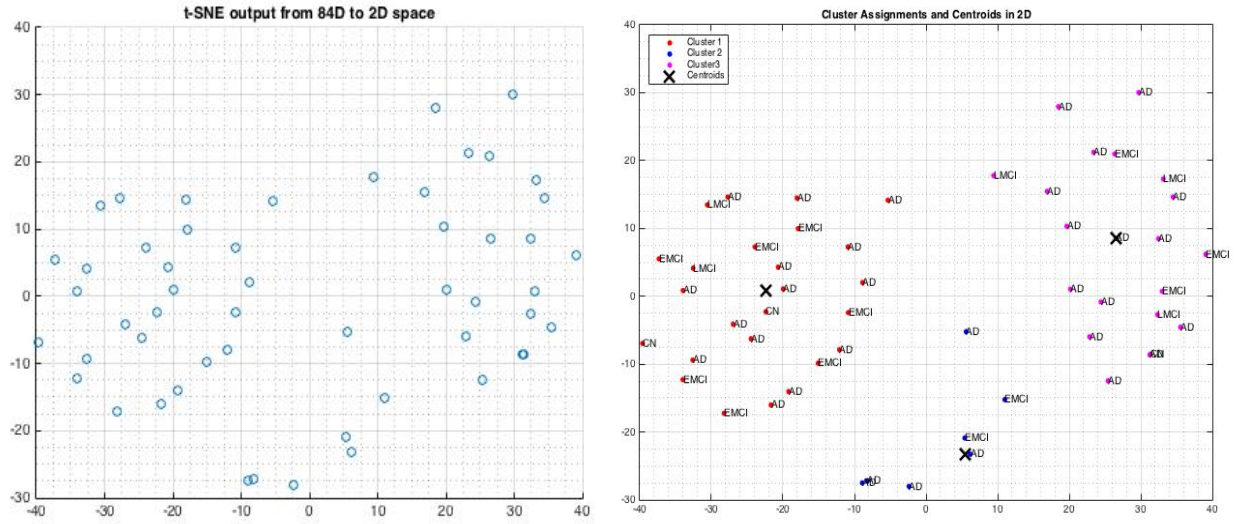

Figure 5.5a (top left): Principal eigenmodes plotted in 2D space after running t-SNE algorithm
Figure 5.5b (top right): Output of *k*-means clustering on t-SNE-reduced eigenmodes with *k*=3 in 2D
Figure 5.5c (bottom): Output of *k*-means clustering on t-SNE-reduced eigenmodes with *k*=3 in 3D

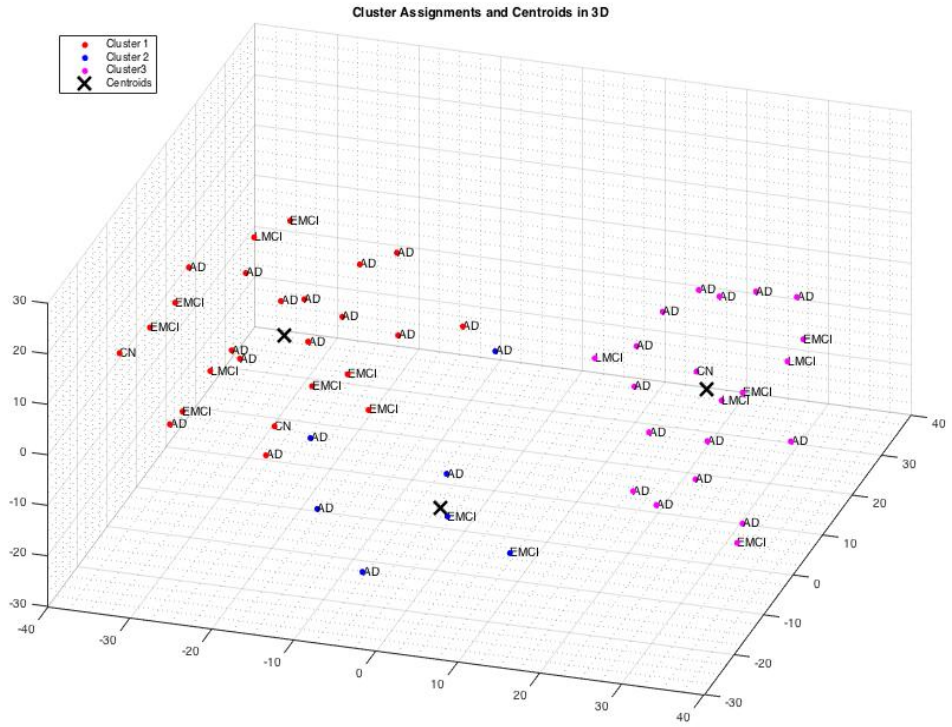

5.6 Anatomical Mapping

Having applied dimensionality reduction followed by *k*-means clustering, each principal eigenmode now belongs in one of three clusters. Intuitively, each cluster of principal eigenmodes represents a specific subnetwork, so the number of clusters corresponds to the number of subnetworks. The number of subnetworks identified here may be limited by the number of subjects, number of ROIs, number of time points, and precision of the various tools in the workflow used to obtain the volumetric measurements, including MRI resolution and accuracy of longitudinal processing. Plotting the original 84 principal eigenvectors (each of 84x1 dimension) by their new cluster labels reveals clear characteristic patterns across the ROIs and thus a distinct shape for each subnetwork. In each of these plots in Figures 5.6a, 5.6b, and 5.6c, individual lines represent single subject principal eigenmodes.

Also included with each respective plot in Figures 5.6a, 5.6b, and 5.6c is the anatomical mapping of each eigenmode cluster onto the brain. For each cluster, the principal eigenmodes belonging to that cluster were averaged to create a single eigenvector. Each value in the eigenvector corresponds to an ROI and each ROI has a known center of mass coordinate position with respect to a map of the brain. For each brain image, the size of the spheres corresponds to magnitude of the eigenmode at a given ROI, and the spheres are color-coded by ROI anatomical region. Frontal, occipital, parietal, subcortical, and temporal map to the integer range [1-5] respectively. These anatomical maps were generated with BrainNet Viewer 1.3 [18].

Looking at the lobular prominence for each principal eigenmode group, the results remain in line with previously theorized AD spread pattern. The subnetwork represented by cluster 1 (Figure 5.6a) is dominated by frontotemporal brain connections and the subnetwork represented by cluster 2 (Figure 5.6b) is localized mainly in the occipital lobe and medial temporal regions. This is in line with the expected afflicted areas in full-blown AD. Cluster 3 is more diverse, revealing a subnetwork

that spans all of the cortical and subcortical regions, with relative sparing of parietal and motor cortices. There may be more underlying subnetworks within the third cluster that are not definitively characterizable due to the limitations mentioned earlier.

Figures 5.6a, 5.6b, & 5.6c (top, middle & bottom): 3D and anatomical plots of principal eigenmode groups defined by *k*-means clusters. The left side of each figure is a 3D line plot of principal eigenmode values with each line representing a single subject. The right side shows the average of these principal eigenmode groups, mapped onto brain anatomy. Colors on the left-side plots represent eigenmode magnitude while color range [1-5] on the right-side brain figures represent the different lobular regions of the ROIs - frontal, occipital, parietal, subcortical, and temporal, respectively.

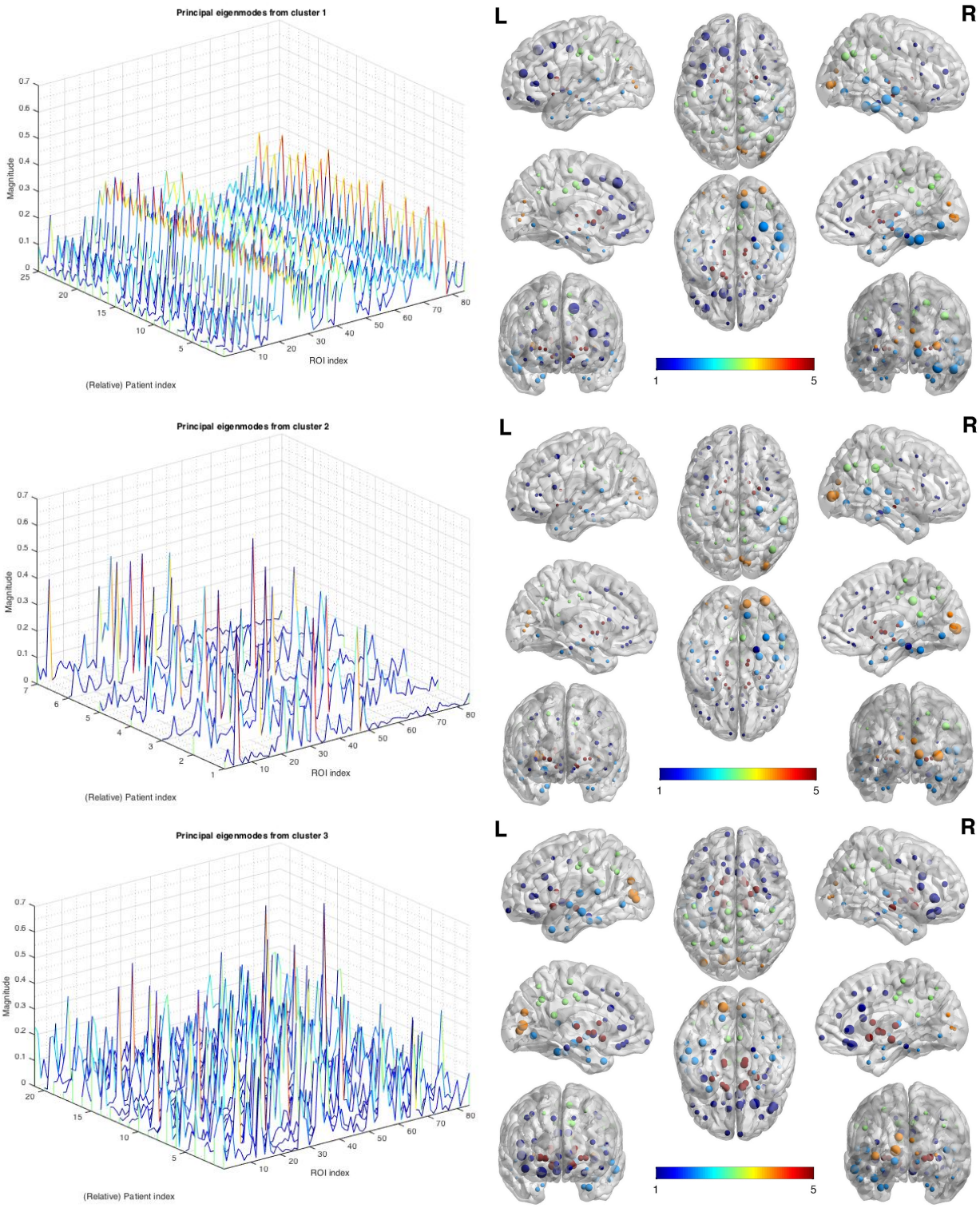

6 Summary & Conclusions

In this study a proposed model for the spread of Alzheimer's disease pathology is evaluated and further researched upon. The "network diffusion" model, published by Raj et al. (2015), relies on both a mathematical foundation based on heat diffusion as well the structural connectivity information for a given patient. This paper applies related methods in order to help characterize the subnetworks that influence AD progression and neural degeneration. Using MRI data from the ADNI project, a cohort of 53 patients is analyzed and dominating networks related to the disease pathology are extracted. Additionally, the limitations of previously published results are evaluated and improved upon.

The response of the network diffusion model is determined in part by the baseline grey matter volume measurements and the eigen decomposition of subject connectomes. Applying PLS to this response allows the eigenmodes or subnetworks of the subject to be identified. The notion of principal eigenmodes, that only one or a few eigenmodes dominate the spread of the disease, is justified by evaluating the histograms of both the PLS coefficients and the PLS eigenvalue indices. These principal eigenmodes or subnetworks represent those pathways most favored by the disease.

ROI-based evaluation strongly supports the presence of patterns amongst the principal eigenmodes. In order to further characterize these subnetworks, the eigenmodes need to be classified or categorized by some means. Employing a combination of dimensionality reduction using t-SNE and classification via *k*-means, for the cohort considered, three strongly distinct clusters of eigenmode patterns are identified. When mapped onto the anatomical regions of the brain, the regions these subnetworks dominate coincide with the areas observed to be heavily affected by severe AD.

6.1 Limitations & Future Work

The predictive ability of a diffusion-model-based approach and the mathematical analysis showed here has yet to be fully evaluated. The number of subjects investigated was limited due to lack of longitudinal data. Those that did possess longitudinal data had varying sets of time points, and even though software correction and post-processing were used, variations between scan sessions, as well as aggregation of computational error from image processing may have polluted the input data to a certain extent. The number of ROIs considered also influenced the granularity of the results, and PLS, t-SNE, and *k*-means all have various counterpart algorithms that may have affected the observed outcome.

Nevertheless, there is a clear path for future work. There is a strong case for the presence of subnetworks in AD disease progression and further break down and extraction of these subnetworks is a natural continuation of this investigation. Here only grey matter volume measurements are considered; a natural extension would include multimodal imaging measures to capture in further detail both the structural and functional brain changes and spread in AD spectrum. The results here are limited by the precision of how the fiber tracts and connections are represented – an in-depth derivation and analysis of individual subject connectome data is warranted.

Another important question that arises is how these subnetworks relate to patient phenotype and other patient-specific characteristics. None of the subject characteristics other than the brain imaging data were considered (e.g. gender, age, education, genotype, depressive symptoms, cardiovascular health, etc.). Furthermore, the implications of identifying subnetworks for AD may find themselves generalizable to other neurodegenerative diseases. When these critical factors can be combined to form a comprehensive model, the ultimate end goal would be to build a classifier for disease state and progression given any patient scan and connectome data.

7 References

[1] Abdi, H. (2010). Partial least square regression, projection on latent structure regression, PLS-Regression. *Wiley Interdisciplinary Reviews: Computational Statistics*, 2, 97-106.

[2] Abdi, H. (2007). Partial least square regression (PLS regression). In N.J. Salkind (Ed.): *Encyclopedia of Measurement and Statistics.* Thousand Oaks (CA): Sage. pp. 740-744.

[3] Aisen, PS et al. "Clinical Core of the Alzheimer's Disease Neuroimaging Initiative: Progress and Plans." *Alzheimer's & dementia : the journal of the Alzheimer's Association* 6.3 (2010): 239–246. *PMC*. Web. 18 Aug. 2016.

[4] Basser P.J., Mattiello J., LeBihan D. MR diffusion tensor spectroscopy and imaging. Biophys. J. 1994;66(1):259–267.

[5] "Dementia Fact sheet N°362". World Health Organization. March 2015. Archived from the original on 18 March 2015. Retrieved 18 Aug. 2016.

[6] Isik, Ahmet Turan. "Late Onset Alzheimer's Disease in Older People." *Clinical Interventions in Aging* 5 (2010): 307–311. *PMC*. Web. 18 Aug. 2016.

[7] Jahanshad N., Lee A.D., Barysheva M., McMahon K.L., de Zubicaray G.I., Martin N.G., Wright M.J., Toga A.W., Thompson P.M. Genetic influences on brain asymmetry: a DTI study of 374 twins and siblings. Neuroimage. 2010;52(2):455–469.

[8] Jucker, Mathias, and Lary C. Walker. "Pathogenic Protein Seeding in Alzheimer's Disease and Other Neurodegenerative Disorders." *Annals of neurology* 70.4 (2011): 532–540. *PMC*. Web. 29 Aug. 2016.

[9] Krishnan, A., Williams, L.J., McIntosh, A.R., & Abdi, H. (2011). Partial Least Squares (PLS) methods for neuroimaging: A tutorial and review. *NeuroImage*, 56, 455-475.

[10] Leow A.D., Yanovsky I., Chiang M.C., Lee A.D., Klunder A.D., Lu A., Becker J.T., Davis S.W., Toga A.W., Thompson P.M. Statistical properties of Jacobian maps and the realization of unbiased large-deformation nonlinear image registration. IEEE Trans. Med. Imaging. 2007;26(6):822–832.

[11] Nir, Talia M. et al. "Effectiveness of Regional DTI Measures in Distinguishing Alzheimer's Disease, MCI, and Normal Aging." NeuroImage : Clinical 3 (2013): 180–195. PMC. Web. 4 June 2016.

[12] Raj, Ashish, Eve Locastro, Amy Kuceyeski, Duygu Tosun, Norman Relkin, and Michael Weiner. "Network Diffusion Model of Progression Predicts Longitudinal Patterns of Atrophy and Metabolism in Alzheimer's Disease." *Cell Reports* 10.3 (2015): 359-69. Web.

[13] Raj, Ashish, Amy Kuceyeski, and Michael Weiner. "A Network Diffusion Model of Disease Progression in Dementia." *Neuron* 73.6 (2012): 1204-215. Web.

[14] Reuter, Martin, Nicholas J. Schmansky, H. Diana Rosas, and Bruce Fischl. "Within-subject Template Estimation for Unbiased Longitudinal Image Analysis." *NeuroImage* 61.4 (2012): 1402-418. Web.

[15] Su, J.H., Deng, G., and Cotman, C.W. (1997). "Transneuronal degeneration in the spread of Alzheimer's disease pathology: immunohistochemical evidence for the transmission of tau hyperphosphorylation.".*Neurobiol*. 4 (5): 365–375. doi:10.1006/nbdi.1997.0164. PMID 9440125

[16] Tobias, Randy D. "An Introduction to Partial Least Squares Regression." *SpringerReference* (1995): n. pag. SAS Institute Inc. Web. <http://www.ats.ucla.edu/stat/sas/library/pls.pdf>.

[17] van der Maaten, L.J.P.; Hinton, G.E. (Nov 2008). "Visualizing High-Dimensional Data Using t-SNE" (PDF). *Journal of Machine Learning Research* 9: 2579–2605.

[18] Xia M, Wang J, He Y (2013) BrainNet Viewer: A Network Visualization Tool for Human Brain Connectomics. PLoS ONE 8: e68910

Publishing Agreement

It is the policy of the University to encourage the distribution of all theses, dissertations, and manuscripts. Copies of all UCSF theses, dissertations, and manuscripts will be routed to the library via the Graduate Division. The library will make all theses, dissertations, and manuscripts accessible to the public and will preserve these to the best of their abilities, in perpetuity.

Please sign the following statement:

I hereby grant permission to the Graduate Division of the University of California, San Francisco to release copies of my thesis, dissertation, or manuscript to the Campus Library to provide access and preservation, in whole or in part, in perpetuity.

Author Signature  Date 9/2/16